Journal of Geophysical Research: Oceans

RESEARCH ARTICLE
10.1029/2018JC013800

A Numerical Study of Interannual Variability in the North Icelandic Irminger Current

Jian Zhao[1,2], Jiayan Yang[1], Stefanie Semper[3], Robert S. Pickart[1], Kjetil Våge[3], Hedinn Valdimarsson[4], and Steingrímur Jónsson[4,5]

[1]Woods Hole Oceanographic Institution, Woods Hole, MA, USA, [2]Horn Point Laboratory, University of Maryland Center for Environmental Science, Cambridge, Maryland, USA, [3]Geophysical Institute, University of Bergen and Bjerknes Centre for Climate Research, Bergen, Norway, [4]Marine and Freshwater Research Institute, Reykjavík, Iceland, [5]University of Akureyri, Akureyri, Iceland

Key Points:
- Waters over the north Icelandic shelf and shelf break exhibit strong seasonal variations in both velocity and hydrographic properties
- The largest interannual change in past two decades occurred in 2003 when the Atlantic Water around Iceland increased volume flux of about 50%
- The wind stress southwest of Iceland is predominantly responsible for such interannual changes in the Atlantic Water transport and salinity

Correspondence to:
J. Zhao,
jianzhao@umces.edu

Citation:
Zhao, J., Yang, J., Semper, S., Pickart, R. S., Våge, K., Valdimarsson, H., & Jónsson, S. (2018). A numerical study of interannual variability in the North Icelandic Irminger Current. *Journal of Geophysical Research: Oceans*, *123*, 8994–9009. https://doi.org/10.1029/2018JC013800

Received 15 JAN 2018
Accepted 8 OCT 2018
Accepted article online 11 OCT 2018
Published online 12 DEC 2018

Abstract The North Icelandic Irminger Current (NIIC) is an important component of the Atlantic Water (AW) inflow to the Nordic Seas. In this study, both observations and a high-resolution (1/12°) numerical model are used to investigate the seasonal to interannual variability of the NIIC and its forcing mechanisms. The model-simulated velocity and hydrographic fields compare well with the available observations. The water mass over the entire north Icelandic shelf exhibits strong seasonal variations in both temperature and salinity, and such variations are closely tied to the AW seasonality in the NIIC. In addition to seasonal variability, there is considerable variation on interannual time scales, including a prominent event in 2003 when the AW volume transport increased by about 0.5 Sv. To identify and examine key forcing mechanisms for this event, we analyzed outputs from two additional numerical experiments: using only the seasonal climatology for buoyancy flux (the momentum case) and using only the seasonal climatology for wind stress (the buoyancy case). It is found that changes in the wind stress are predominantly responsible for the interannual variations in the AW volume transport, AW fraction in the NIIC water, and salinity. Temperature changes on the shelf, however, are equally attributable to the buoyancy flux and wind forcing. Correlational analyses indicate that the AW volume transport is most sensitive to the wind stress southwest of Iceland.

Plain Language Summary The Irminger Current is an important component for the large-scale ocean circulation in the subpolar North Atlantic. The Irminger Current splits one branch that flows northward on the eastern side of the Denmark Strait. This branch further penetrates onto the Icelandic shelf and is named as North Icelandic Irminger Current (NIIC). The NIIC carries relatively warm, salty, and high nutrient Atlantic Water, so that it is vital for the local climate and ecosystem. This study investigates the changes of NIIC on interannual time scale, particularly for a prominent event in 2003. The Atlantic Water trapped in the NIIC was increased by more than 50% during this event. Numerical modeling experiments were performed to identify and examine the key processes for this event. The wind forcing southwest of Iceland was found to be the dominant driver for the 2003 event, especially for the increased Atlantic Water volume transport. The findings have important implications for understanding the mechanisms of poleward heat transport variability and biologic productivity near Iceland, a key region that connects the subpolar North Atlantic Ocean and Arctic-Subarctic Seas.

1. Introduction

The transport of warm and saline Atlantic Water (AW) over the Greenland-Scotland Ridge (GSR) into the Nordic Seas is an essential component of the Atlantic Meridional Overturning Circulation (Dickson et al., 2008; Hansen et al., 2008). The transport of AW is distributed among three branches across the GSR: about 0.88 Sv through the Denmark Strait, about 3.80 Sv between Iceland and the Faroe Islands, and about 2.70 Sv through the Faroe-Shetland Channel (FSC, Berx et al., 2013; Hansen et al., 2015; Jónsson & Valdimarsson, 2012; Østerhus et al., 2005). The AW inflow results in considerable fluxes of heat, salt, and nutrients into the Nordic Seas and ultimately the Arctic Ocean, affecting the high-latitude climate, water transformation, and ecosystem (Dickson & Brown, 1994; Dickson et al., 2008; Hansen & Østerhus, 2000; Hansen et al., 2003, 2008, 2010, 2015).

The northward transport of the AW through the Denmark Strait occurs mainly via the North Icelandic Irminger Current (NIIC), whose origin can be traced to the Irminger Current in the subpolar North Atlantic

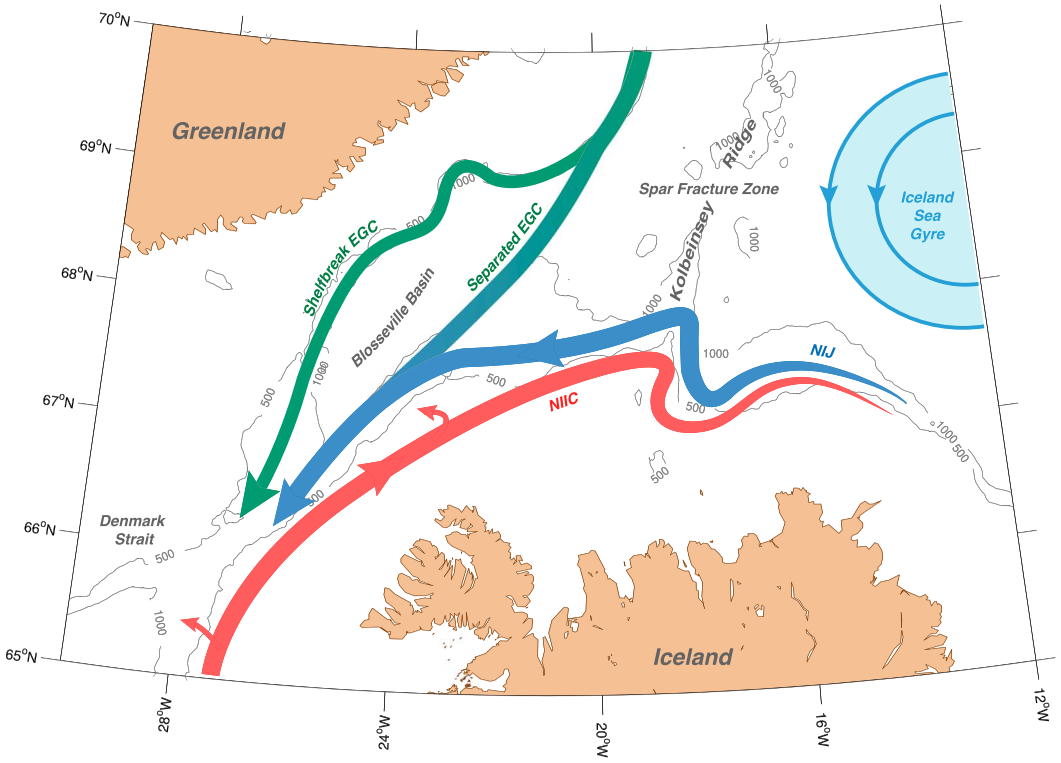

Figure 1. Schematic circulation in the region north of Denmark Strait and geographic place names, after Våge et al. (2013). The 500- and 1,000-m isobaths are contoured in gray. EGC = East Greenland Current; NIIC = North Icelandic Irminger Current; NIJ = North Icelandic Jet.

Ocean. The NIIC flows northward on the eastern side of the Denmark Strait (Figure 1). The warm and saline AW in the NIIC meets the cold and low-salinity Polar Water (PW) off Iceland's northwest coast. A mixture of AW and PW is further fluxed onto the north Icelandic shelf. The NIIC, even with a relatively small volume transport, is also a main source of heat and salt to the Iceland Sea and thus strongly influences convective processes there. Våge et al. (2011) suggested that the AW in the NIIC is transported offshore by eddies and cooled by wintertime air-sea fluxes to form a dense water mass that feeds the North Icelandic Jet—an upstream branch of the Denmark Strait Overflow. The existence of this local overturning loop has been supported by numerical simulations (Behrens et al., 2017). North of Iceland the NIIC continues to flow anticyclonically over the outer part of the shelf. The flow is favorable for the migration of larval cod from the main spawning grounds south of Iceland to the nursery regions on the north Icelandic shelf (Jónsson & Valdimarsson, 2005). The relatively high nutrient content in the AW is also important for primary productivity around Iceland (Thordardottir, 1984).

Given the importance of the NIIC to the local climate and ecosystem, considerable efforts have been devoted to monitor the NIIC variability using both ships and long-term moorings. At the Hornbanki section on the north Icelandic shelf, a well-maintained mooring array has been continuously measuring the NIIC since 1994 (see Figure 2 for the location of the array). As a result, the mean structure and variations of the current are well documented at that location (e.g., Jónsson & Valdimarsson, 2005, 2012; Østerhus et al., 2005). The long-term mean volume flux of AW in the NIIC has been estimated to be 0.88 Sv and displays substantial variability on multiple time scales (Jónsson & Valdimarsson, 2012). In addition, the NIIC volume transport has been shown to covary with the transports of the other two branches of the AW inflow. For instance, a negative correlation between the NIIC and the FSC transports was detected in both model and observational data (Nilsen et al., 2003; Østerhus et al., 2005).

Among the three branches of the AW inflow to the Nordic Seas, the NIIC is by far weakest in terms of volume transport and arguably the least studied (e.g., Nilsen et al., 2003; Olsen & Schmith, 2007; Richter et al., 2009; Sandø et al., 2012). There remains considerable uncertainty regarding the processes and mechanisms that are

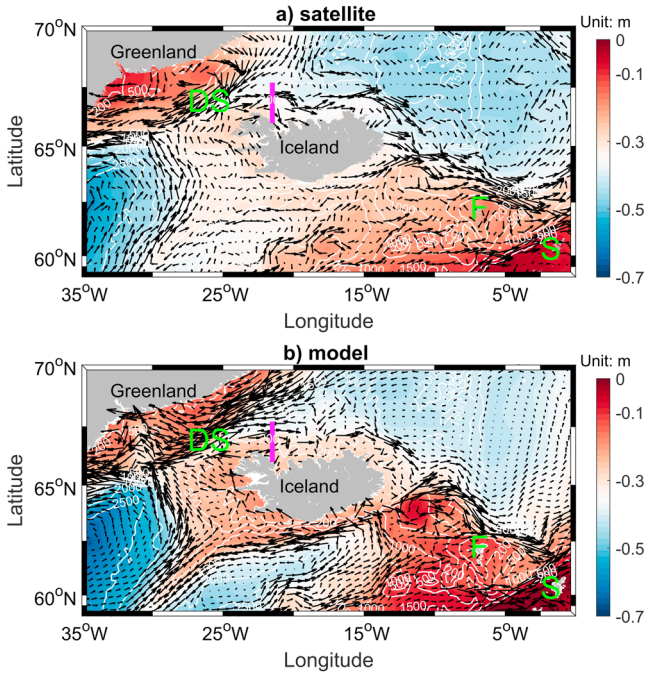

Figure 2. Mean surface geostrophic circulation from satellite altimetry observations and the HYCOM control experiment. (a) The long-term mean (1993–2015) absolute dynamic topography (ADT) observed by the satellite altimetry (color). (b) The mean sea surface height simulated by HYCOM. The surface geostrophic currents calculated from altimetry and HYCOM are shown by the gray vectors. The bathymetric contours (white lines) indicate isobaths of 200, 500, 1,000, 1,500, 2,000, and 2,500 m. DS denotes Denmark Strait. F and S represent the Faroe and Shetland Islands, respectively. The magenta line denotes the Hornbanki section. HYCOM = HYbrid Coordinate Ocean Model.

responsible for its variability. To date, several mechanisms have been identified that appear to influence the overall transport of the AW across the GSR, including wind-induced wave propagation from the Atlantic Ocean into the Nordic Seas (Orvik & Skagseth, 2003; Sandø & Furevik, 2008), local wind forcing driving the transport in the FSC (Richter et al., 2012; Sherwin et al., 2008), and the AW inflow compensating the overflow (Hansen et al., 2010; Sandø et al., 2012). Among these processes, the large-scale wind forcing, especially the North Atlantic Oscillation (NAO), has been shown to play a key role (Nilsen et al., 2003; Olsen & Schmith, 2007; Richter et al., 2009). In addition, changes in the pattern and strength of the subpolar gyre have also been linked to the AW transport into the Nordic Seas (Hátún et al., 2005; Häkkinen et al., 2011).

The seasonal cycle for the AW transport in the NIIC is distinct, with a minimum in late spring and maximum in summer (Jónsson & Valdimarsson, 2012). This seasonal variability is considerably different from that in the FSC and IF. For instance, the AW inflow in the IF is strong in early spring and weak in late summer to early fall (Hansen et al., 2008). This indicates that the dynamics for the NIIC may be different from the other two branches. The model simulations of Logemann and Harms (2006) indicated that most high frequency (time scales ranging from days to months) and seasonal NIIC variability are linked to the local wind around Iceland. It is unclear whether the same processes and forcing are responsible for interannual variability, such as the large anomalous transport observed in 2003 (Jónsson & Valdimarsson, 2012). The measurements analyzed by Logemann and Harms (2006) spanned the period between May 1997 and June 2002 and therefore excluded the anomalous event in 2003.

This study investigates the structure and variability of the NIIC using a high-resolution (1/12°) numerical model. We focus on the interannual variability in the NIIC and especially a prominent event in 2003. Several model runs are designed to separate the relative contributions from wind stress and buoyancy forcing to the interannual variability. The model setup, including the boundary conditions and forcing fields, is explained in section 2. The model simulations and analyses are presented and discussed in section 3. Further discussion and a summary are then presented in section 4.

2. Data and Model

2.1. Observations

The mooring data used in this study come from a series of deployments of the Hornbanki array (Figure 2) since 1994. The array was configured to sample the NIIC core and consisted of one mooring between 1994 and 1999 and three moorings most of the time after 1999. The velocity in the upper 200 m was measured by either current meters or acoustic Doppler current profilers, and the temperature was observed by thermistors at 80 and 150 m. The reader is referred to Jónsson and Valdimarsson (2012) for more detailed descriptions of the mooring configuration, instrumentation, and data acquisition. Here we use the AW transport time series, which is the fraction of the total transport associated with the warm and salty AW, computed using an end-member analysis (see Jónsson and Valdimarsson, 2012 for details).

The shipboard data come from a series of 10 high-resolution occupations of the Hornbanki section that included both conductivity-temperature-depth (CTD) measurements and lowered acoustic Doppler current profiler (LADCP) measurements. In all instances the CTD conductivity data were calibrated using in situ water samples, and the LADCP data were detided. The reader should consult Pickart et al. (2017) for details of this, including measurement accuracies. The occupations occurred in October 2008; August 2009 and 2010; February 2011; September 2011; February 2012; and August 2012, 2013, 2015, and 2017. We constructed mean vertical sections of potential temperature, salinity, and absolute geostrophic velocity (perpendicular

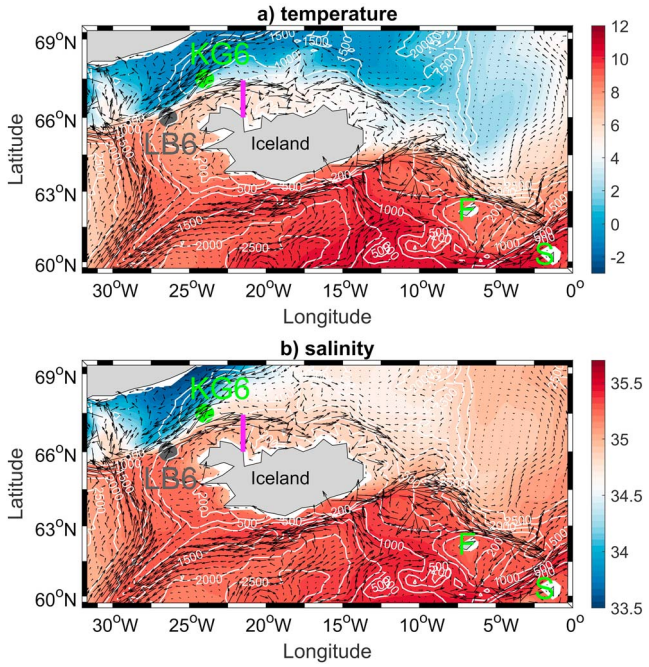

Figure 3. Mean fields at 110 m simulated by HYCOM for (a) temperature (°C) and (b) salinity. The LB6 (station 6 on the Látrabjarg transect) and KG6 (station 6 on the Kögur section) sites are indicated. These are the AW and PW end-member locations (see text). Isobaths (white contours) are the same as in Figure 2. HYCOM = HYbrid Coordinate Ocean Model; AW = Atlantic Water; PW = Polar Water.

to the section; since the section is oriented north-south, the absolute geostrophic velocity is zonal.) to be compared with the model output.

Satellite data are used to further validate the model and to supplement our analyses. They include the absolute dynamic topography (ADT) and surface geostrophic velocity fields between 1992 and 2015. The Ssalto/Duacs altimeter products are produced and distributed by the Copernicus Marine and Environment Monitoring Service (http://www.marine.copernicus.eu).

2.2. Numerical Model

Numerical simulations were performed using an eddy-resolving high-resolution (1/12°) configuration of the HYbrid Coordinate Ocean Model (HYCOM). The model was originally configured by Xu et al. (2010) and used in several studies in both the Atlantic Ocean and Nordic Seas (Xu et al., 2010, 2012, 2013). The model domain spans from 28°S to 80°N and has 32 vertical layers. The horizontal resolutions range from 3 to 5 km in the subpolar North Atlantic. Along the northern and southern boundaries we apply a no-normal flow condition in the velocity field and restore the temperature and salinity to their monthly climatological fields. Further details of the model setup were explained by Xu et al. (2010, 2012).

The 1/12° HYCOM simulations were found to successfully reproduce both the long-term mean and variations of the subpolar North Atlantic circulation, particularly the Atlantic Meridional Overturning Circulation, the boundary currents in the Labrador Sea, and the North Atlantic Current (Xu et al., 2012, 2013). We used the climatological simulation E026 by Xu et al. (2012) as an initial condition, from which our regional HYCOM model was further integrated for 25 years by repeatedly using the daily 1992 atmospheric forcing from National Centers for Environmental Prediction (NCEP) Climate Forecast System Reanalysis (CFSR) data. The CFSR reanalysis was obtained from the atmosphere-ocean-land-ice coupled system with assimilation of satellite radiances. The data set has a global resolution of ~38 km (T382) and a temporal resolution of 6 hr (Saha et al., 2010, 2014). Surface heat flux and wind stress were calculated using the bulk formula of Kara et al. (2005) with input variables from CFSR. Freshwater flux was obtained directly from the CFSR data set.

After this 25-year spin-up, three experiments were performed. In the *control* run, the HYCOM was integrated from 1992 to 2015 with daily forcing fields from NCEP-CFSR. In the *momentum* run, the HYCOM was forced by climatological buoyancy flux but interannually varying momentum fluxes. In the *buoyancy* run, the model was driven by climatological momentum flux and interannually varying buoyancy flux. The two sensitivity experiments are designed to evaluate the relative contribution from each forcing field—buoyancy and wind stress—to the interannual variations of the NIIC.

3. Results

3.1. Mean and Seasonal Cycle

The HYCOM control experiment reproduces reasonably well the spatial pattern for the near-surface circulation in the subpolar North Atlantic (Figure 2). In addition to the gyre-scale topographic-following cyclonic circulation and the East Greenland Current, the model also fully captures the three AW inflow branches to the Nordic Seas in the FSC, over the Iceland-Faroe Ridge, and in the eastern part of the Denmark Strait. The simulated circulation is broadly consistent with that derived from available observations (e.g., Jakobsen et al., 2003; Valdimarsson & Malmberg, 1999). The warm and saline water masses are clearly present along the pathways of the three inflow branches (Figure 3), indicating their origins from the Atlantic Ocean. Once in the Nordic Seas the AW is either transformed to denser water or further transported into the Arctic Ocean.

This study focuses on the NIIC that separates from the Irminger Current in the region to the west of Iceland and flows northward and then eastward over the outer north Icelandic shelf. We now compare the modeled

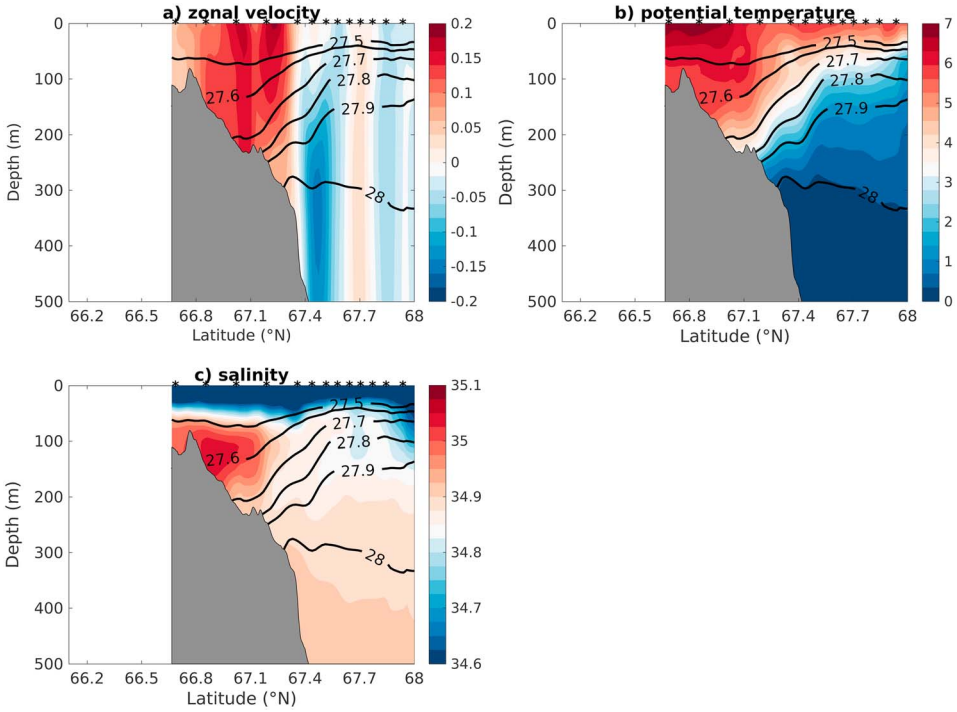

Figure 4. Mean vertical sections along the Hornbanki section from the observations. (a) Zonal velocity (unit: m/s), (b) temperature (unit: °C), and (c) salinity (unit: Practical Salinity Scale 1978). The potential density (σ_θ, unit: kg/m^3) is denoted by black contours. The velocity is measured by the LADCP, and the hydrography is from the CTD profiles. The average positions of the CTD stations are indicated by asterisks. The average station distance is about 18.5 km on the shelf and about 8 km offshore of the shelf break. LADCP = lowered acoustic Doppler current profiler; conductivity-temperature-depth.

NIIC at the Hornbanki section to the CTD and LADCP observations collected there. The measured velocity field along the Hornbanki section indicates that the shelf region with water depths shallower than 300 m is occupied by eastward flow (Figure 4a). The eastward current has a strong barotropic component inshore of the shelf break with significant flow extending from the surface to the bottom. Farther offshore, there is a branch of westward flow toward the Denmark Strait centered near the 600-m isobath. This is the North Icelandic Jet, which transports overflow water denser than σ_θ = 27.8 kg/m^3 (see also Jónsson, 1999; Jónsson & Valdimarsson, 2004; Pickart et al., 2017; Våge et al., 2011).

The model output, subsampled to the cruise periods, shows a well-defined eastward jet near the shelf break where the density front is located (Figure 5a). Although the observed eastward flow has a wider meridional extent than the model result, they yield a similar volume transport for the NIIC (discussed below). The numerical results also reveal another branch of eastward flow in the coastal region, but we cannot confirm its existence because the velocity observations are not available south of 66.7°N. It should be mentioned that the long-term mean fields, averaged over all monthly model outputs between 1992 and 2015, are very similar and not shown here. As such, the fields displayed here accurately reflect the long-term pattern.

The warm and salty AW can be easily identified between the coast and shelf break in both the observations and model (Figures 4 and 5). A layer of low salinity water is located near the surface, likely due to the fact that most cruises were performed in summer. The front between the AW and the colder and fresher water offshore is bounded by the σ_θ levels 27.6 and 27.9 and is collocated with the eastward flow. Following the method employed by Jónsson and Valdimarsson (2012) and Pickart et al. (2017), we computed the AW fraction across the Hornbanki section for the model output. In particular, we chose the AW and PW end-member sites to be at the same geographical locations as those used in the observational studies, denoted by LB6 and KG6, respectively, (LB6 is station 6 on the Látrabjarg line, and KG6 is station 6 on the Kögur line; Jónsson & Valdimarsson, 2012) in Figure 3. The simulated temperature and salinity maps at 110 m indicate that indeed the LB6 site is embedded in the AW, and the water mass at KG6 is characterized by the cold and fresh PW (Figures 3 and 6). Furthermore, the amplitudes of both the seasonal and interannual variations at KG6 are

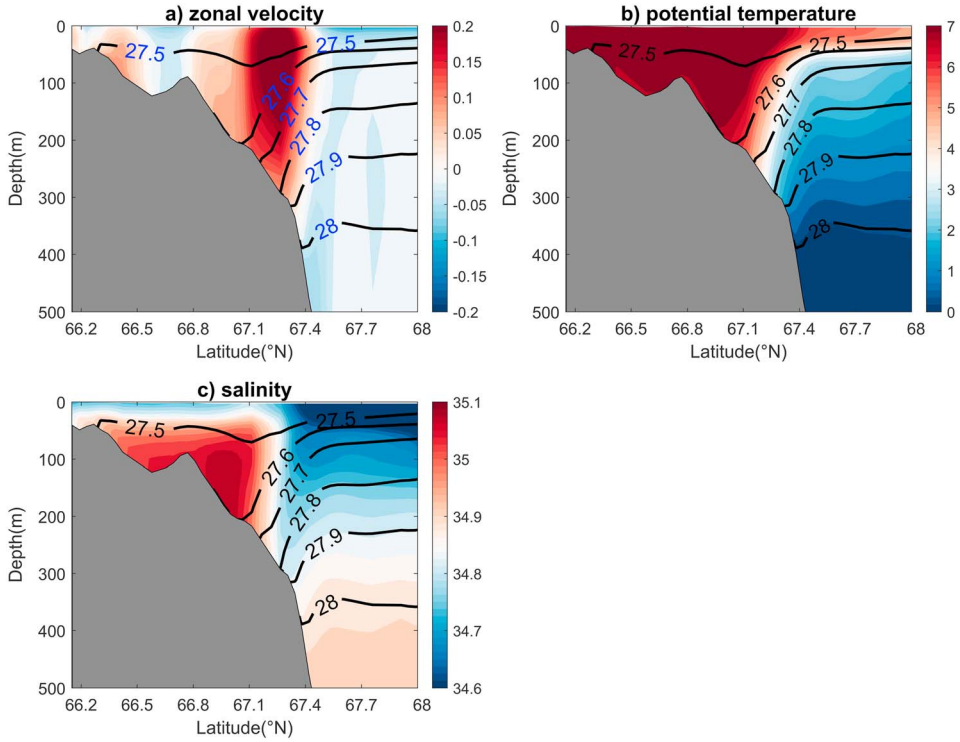

Figure 5. Same as Figure 4 but from the HYCOM control experiment. The model outputs are between 1992 and 2015, and the fields correspond to the cruise periods, except for the shipboard occupation in August 2017. HYCOM = HYbrid Coordinate Ocean Model.

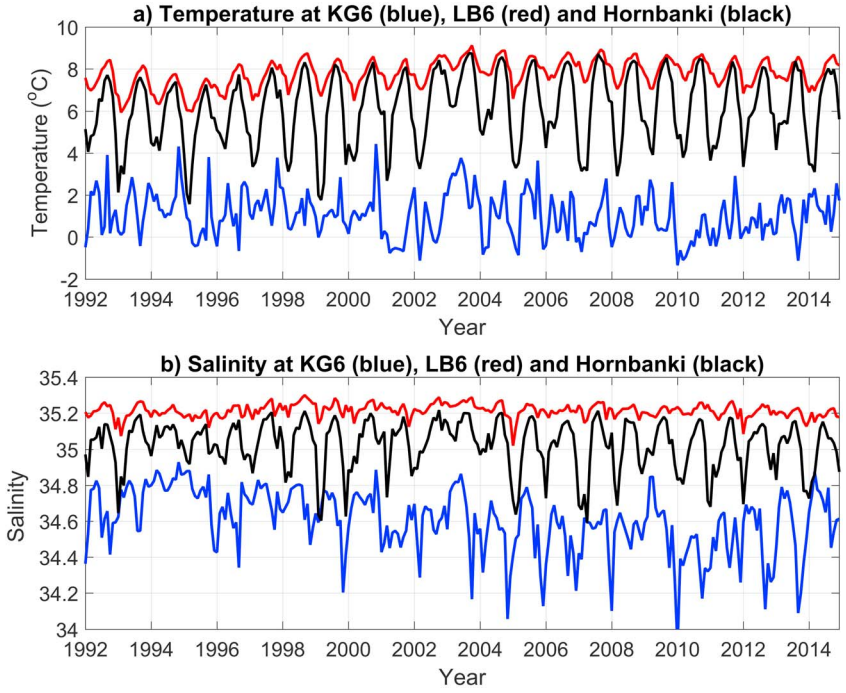

Figure 6. Temperature (a) and salinity (b) at 110 m for the LB6 (red) and KG6 (blue) stations in the HYCOM control run. The black lines denote the temperature and salinity at 110 m at the Hornbanki section (67°N). HYCOM = HYbrid Coordinate Ocean Model.

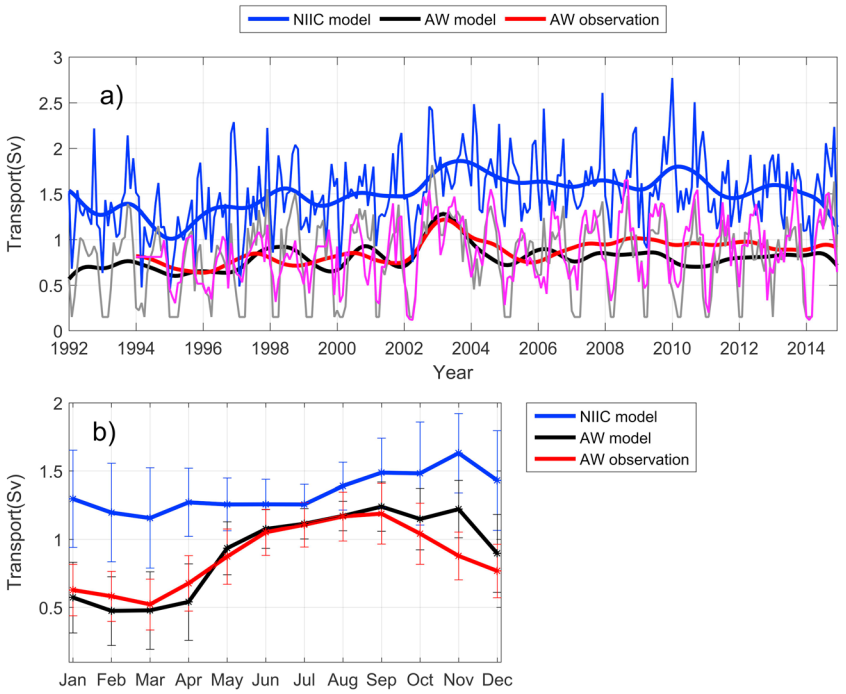

Figure 7. (a) Monthly (blue thin line) and 2-year low-pass filtered (blue thick line) time series for the total model NIIC transport (without being weighted by the AW fraction). Also shown are the monthly AW transports of the NIIC across the Hornbanki section in the HYCOM control experiment (gray thin line) and the observations (magenta thin line). The 2-year low-pass time series are indicated as well (black thick line for HYCOM and red thick line for the observations). (b) Climatological seasonal cycles of the AW transport from HYCOM (black line) and the observations (red line), and that for the total NIIC transport from HYCOM (blue line). The standard deviations are denoted by the thin vertical bars. HYCOM = HYbrid Coordinate Ocean Model; NIIC = North Icelandic Irminger Current; AW = Atlantic Water.

larger than at LB6 (Figure 6), which is consistent with observations (Jónsson & Valdimarsson, 2012). We then computed the fraction of AW at each depth along the Hornbanki section using the corresponding end-member temperature and salinity values at LB6 and KG6. The time-varying end-members were utilized in our calculation. Finally, the AW transport across the Hornbanki section was calculated by multiplying the AW fraction, velocity, and spatial area for each grid cell in HYCOM.

The monthly-averaged total NIIC transport (i.e., all eastward velocity within NIIC, not just the AW portion) for the model time period of 1992–2015 yields a long-term mean value of 1.36 Sv (Figure 7a). Figure 7a also shows the monthly time series of the AW transport in the HYCOM control experiment compared with the observations analyzed by Jónsson and Valdimarsson (2012). The mean modeled AW transport is 0.81 Sv compared to the measured value of 0.88 Sv. The correlation coefficient between the model and data is 0.72, which is significant at the 95% confidence level of Student's *t* test. It is apparent that both the total NIIC transport and AW transport in the model contain substantial seasonal and interannual variabilities. Their monthly values have similar standard deviations (0.40 Sv), which are slightly larger than those from the measurements, 0.34 Sv. In the following, we will examine the variation on seasonal and interannual time scales.

The monthly climatological seasonal cycle for the total simulated NIIC transport, as well as the AW portion, is presented in Figure 7b. The total transport reaches a minimum in late winter and maximum in late fall. However, the AW component has a more pronounced seasonal cycle that peaks earlier in the fall. This is because the seasonal variation of the AW component reflects the changes in both the velocity and the AW fraction. The seasonal range in AW transport is about 0.75 Sv in HYCOM compared to 0.45 Sv for the total NIIC transport. Therefore, the AW fraction is an important factor that modulates the seasonal variation of the AW transport in the NIIC. The percentage of AW along the model section exhibits a minimum of 50% in March and a maximum of 95% in September.

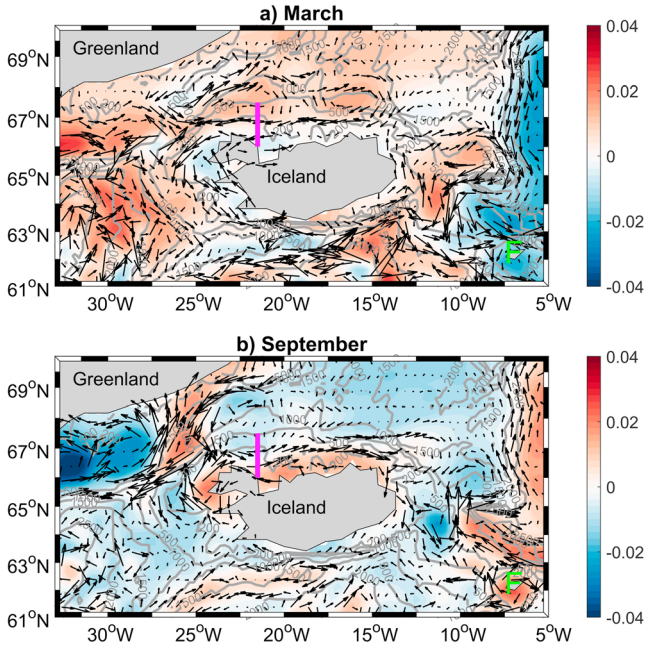

Figure 8. Anomalous absolute dynamic topography (unit: m) constructed from the altimetry data for March (a) and September (b) corresponding to the minimum and maximum months in the climatological seasonal cycle of NIIC transport. The corresponding surface geostrophic current anomalies are indicated by the vectors. Isobaths are denoted by the gray lines. NIIC = North Icelandic Irminger Current.

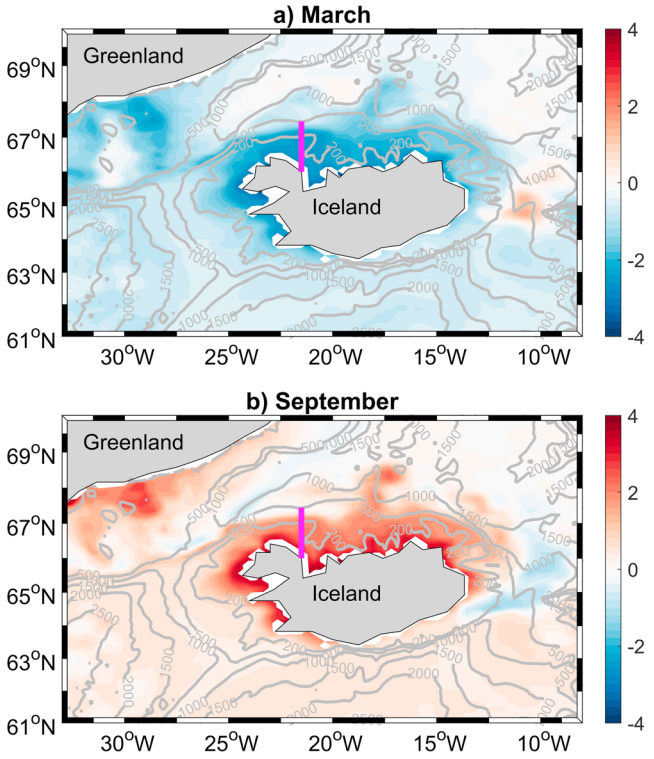

Figure 9. Temperature anomalies (unit: °C) at 110 m in March (a) and September (b) from the climatological cycle in the HYCOM *control* run. Isobaths are denoted by the gray lines. HYCOM = HYbrid Coordinate Ocean Model.

The observed seasonal cycle for the AW transport is similar to that in the HYCOM control experiment (Figure 7b). Both the model and observations show that the minimum transport occurs in late winter and the maximum takes place in early fall. However, there are some differences, most notably that the seasonal range is greater in the model (0.75 Sv in HYCOM compared to 0.68 Sv for the observations) and that the measured AW transport decreases more markedly after September. The difference between the modeled and observed seasonal cycles for the AW properties and transports is likely due to the model's deficiency in representing the mixing between AW and PW. For example, the observed maximum proportion of AW occurs in July with a value of 85% (Jónsson & Valdimarsson, 2012), compared to September with a percentage of 95% in the model. Observational biases may also contribute to the model-data inconsistency. We note that the KB6 and LB6 stations were sampled 4 times annually, and occasionally missing instruments or moorings on the Hornbanki section cause about 10–15% error in the estimation of the AW transport (Jónsson & Valdimarsson, 2012).

The spatial structure associated with the seasonally varying NIIC can be identified from the satellite altimetry data (Figure 8). When the NIIC reaches its minimum and maximum transports in March and September, respectively, the ADT exhibits corresponding negative and positive anomalies along the Iceland coast. The ADT in March is anomalously low over the entire north Icelandic shelf and extends southwestward to about 63.5°N. The ADT away from the shelf has positive anomalies, and this gradient helps set up a westward anomalous geostrophic current. These results suggest that the NIIC seasonality has a broad spatial scale and coherent variability around Iceland. While it is known that biases in the altimetry data are generally higher in coastal waters, the ADT variability identified here is consistent with the seasonal cycle of the NIIC volume transport in both the model and observations.

The horizontal patterns of the temperature and salinity anomalies at 110 m in HYCOM suggest that the North Icelandic shelf has coherent hydrographic changes in March and September (Figures 9 and 10). The peak-to-peak seasonal change has an amplitude of 8 °C in temperature and 0.40 in salinity. The most significant changes mainly occur shoreward of the 200-m isobath, where the mean hydrographic front is located. The seasonal change in velocity at 200 m from HYCOM (not shown) is qualitatively similar to that seen in the surface satellite data. The largest variations in velocity at 200 m are found to be near the temperature and salinity front, suggesting that the heat and salt advection by the NIIC may modulate the intensity of the density front and hence affect the baroclinic current near the shelf break.

The driver for the NIIC seasonal cycle has been attributed mainly to the wind field northeast of Denmark Strait (Logemann & Harms, 2006). The highest monthly mean transport occurs when winds from north are weak, whereas the volume flux is reduced when the northerly winds are intensified (Astthorsson et al., 2007; Jónsson & Valdimarsson, 2005). This correspondence between the NIIC seasonal changes and local winds is also found in our model simulation. Therefore, our results are in line with Logemann and Harms (2006) regarding the main driver of NIIC seasonality.

3.2. Interannual Variability

The interannual variability can be identified either through annual mean or low-pass filter processing. We tried both methods and found that their

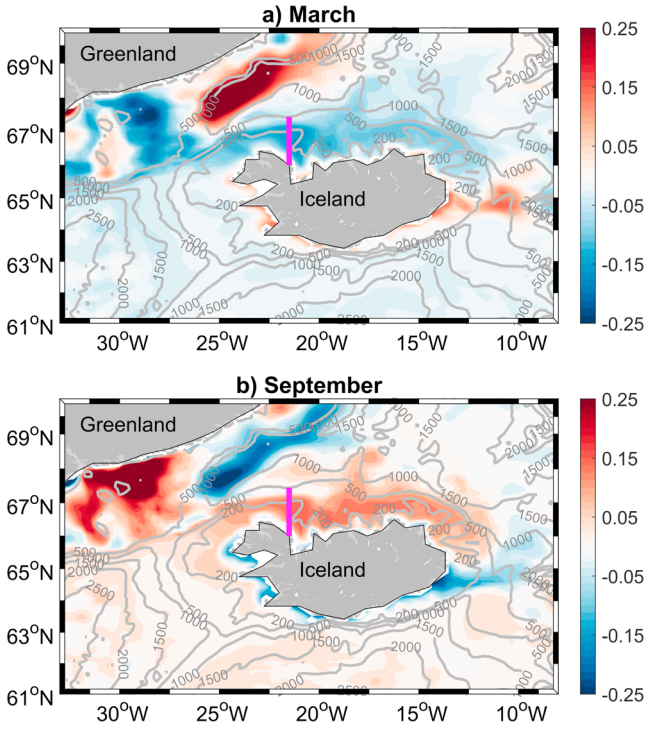

Figure 10. Same as Figure 9 except for salinity anomalies (color shading).

detected interannual fluctuations are similar. Here we only present the results based on a 2-year low-pass filter because it illustrates better the timing for the 2003 event focused on in this study. The effective degree of freedom for the low-pass filtered data is estimated by time-lagged autocorrelation (Santer et al., 2000). The 1-month lag autocorrelation is 0.92 for the filtered data, so that the effective degree of freedom is 12. This value is used to perform statistical evaluations assuming a Student's *t* distribution.

The most prominent change in the NIIC over the last two decades is the increase of the AW transport in 2003 (Figures 7a and 11a). The AW volume transport reached a peak value of 1.30 Sv, significantly above the long-term average transport of 0.88 Sv. The event began in late 2002 and lasted until spring 2003, when the climatological AW volume transport should be seasonally low. This event is well simulated in the control experiment with a relatively high correlation coefficient of 0.67 between the model and observations. In contrast, there is only a small increase in 2003 for the low-pass filtered full NIIC transport (Figure 7a). The different behavior between AW volume transport and full NIIC transport reflects that the AW proportion in NIIC water is the primary factor to produce the 2003 event. The AW proportion reaches about 82% in the model and 76% in observations (Jónsson & Valdimarsson, 2012). For comparison, the proportion of AW for other years is 65–75% in the HYCOM control run and 53–67% in the measurements. Thus, the 2003 event clearly stands out from all other years in both AW volume transport and water mass composition.

The elevated proportion of AW resulted in increases in both temperature and salinity of the NIIC water along the Hornbanki section. This is confirmed by the 2-year low-pass filtered temperature and salinity time series

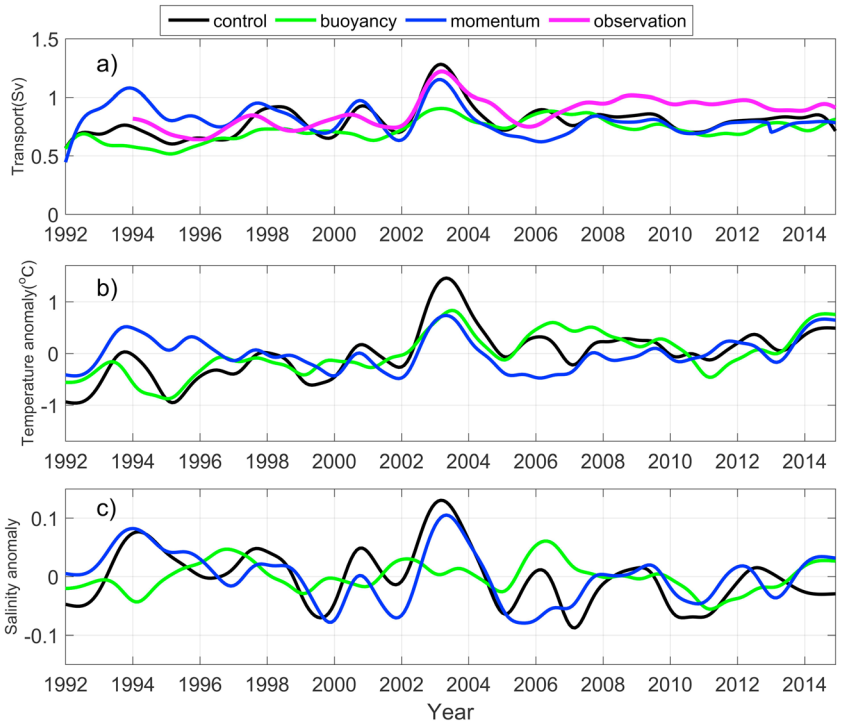

Figure 11. Interannual anomalies of the AW transport (a), temperature (b), and salinity (c) at 110 m along the Hornbanki section in the control (black), buoyancy (green), and momentum (blue) experiments. The observed AW transport is illustrated by magenta line in Figure 11a. AW = Atlantic Water.

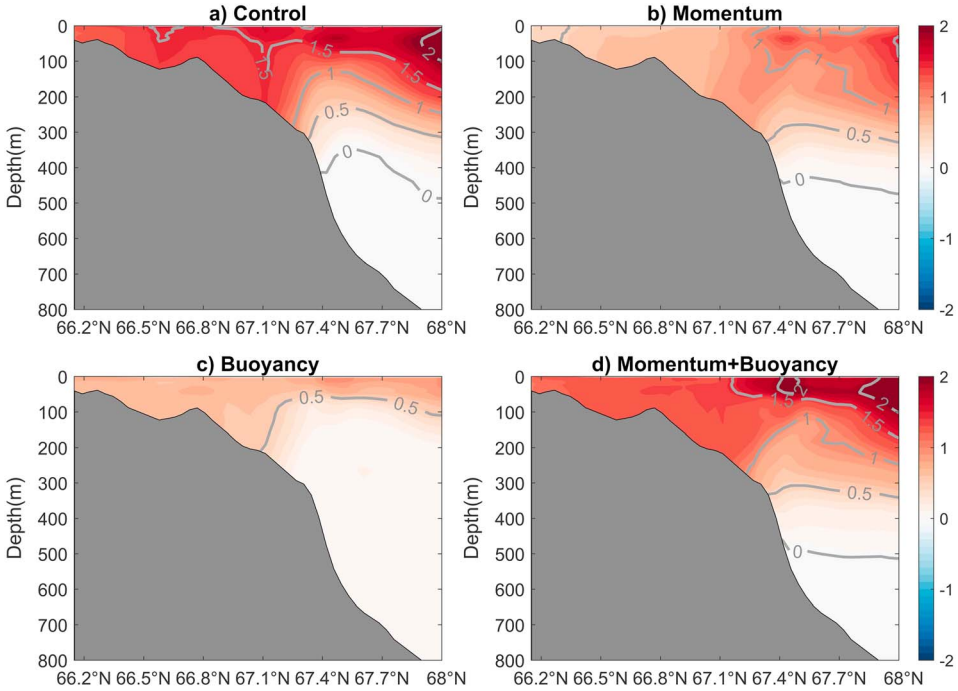

Figure 12. Temperature anomaly for the Hornbanki section in April 2003 when the largest AW transport in the NIIC occurs (unit: °C). The anomaly is calculated from the 2-year low-pass filtered data in *control* (a), *momentum* (b), and *buoyancy* (c) runs. The superposition of the anomalies in momentum and buoyancy experiments is displayed in Figure 12d, which recover the control results. AW = Atlantic Water; NIIC = North Icelandic Irminger Current.

at 110 m at 67°N along the Hornbanki section (black curves in Figures 11b and 11c). The vertical sections for the temperature and salinity anomalies in 2003 indicate that the most prominent changes took place in the upper 200 m (Figures 12a and 13a). Similar anomalies in both temperature and salinity are found at the LB6 station (see Figure 3) where the core AW is located. However, no significant increase in either temperature or

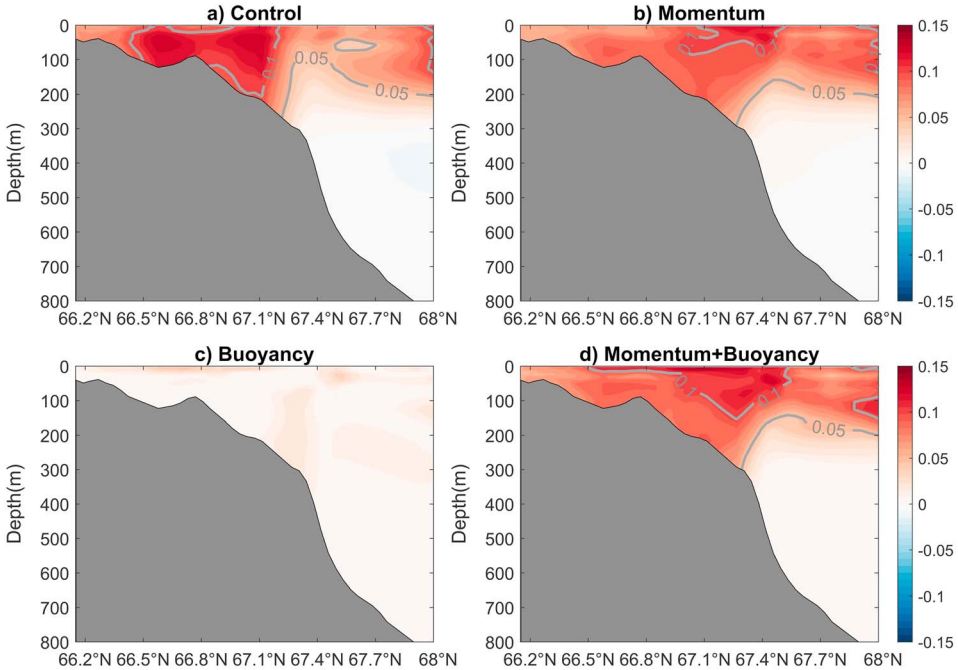

Figure 13. Same as Figure 12 except for the salinity field.

salinity is detected at the KG6 station (see Figure 3), which is predominantly characterized by PW. In addition, the warming event in 2003 was also detected downstream of the Hornbanki section (Jónsson & Valdimarsson, 2012). Therefore, our analyses indicate that changes observed in 2003 at the Hornbanki section resulted from an increased AW transport along the north Icelandic shelf. The characteristics of this event have been well simulated in our control experiment. As such, we are confident that our model is suitable for examining the overall interannual variability.

To identify the causes for the year-to-year changes in the HYCOM control run, outputs from the momentum and buoyancy experiments were analyzed. Note that the seasonal cycles in all three experiments are quite similar because they share the same climatological seasonal forcing. Their differences are due to interannual forcings. The momentum case uses interannually changing wind stress forcing, whereas the buoyancy experiment is forced by interannually varying buoyancy fluxes. The long-term averaged AW transport in the momentum run is about 0.87 Sv, virtually identical to 0.88 Sv in the control experiment. The buoyancy run generates a mean AW transport of 0.78 Sv. The 2-year low-pass filtered AW transport shows that the momentum experiment produces interannual changes that closely resemble the control run (Figure 11a). By contrast, the AW transport in the buoyancy run is relatively steady. Specifically, the intensified AW transport in 2003 reaches a maximum of 1.15 Sv in the momentum experiment but only about 0.90 Sv in the buoyancy run. Therefore, the interannual variations in the AW transport are predominately due to the interannually varying momentum fluxes.

The low-pass filtered temperature time series demonstrate that both the momentum and buoyancy experiments produce a temperature increase in early 2003. In both experiments, the temperature anomalies at 110 m along the Hornbanki section at 67°N are about 0.6–0.7 °C during the 2003 event, which is about half of the 1.4 °C in the control run. Over the whole simulation period from 1992 to 2014, neither experiment alone can account for the overall interannual changes in temperature that were simulated in the control run. The statistical correlation is 0.75 between momentum and control experiments and 0.69 between buoyancy and control runs, both significant at the 95% confidence level.

The temperature anomalies along the Hornbanki section during the maximum AW transport in 2003 show rather different patterns between the momentum and buoyancy experiments (Figure 12). The temperature anomaly in the momentum experiment reveals a localized region of warming near the shelf break that colocates with the core of the NIIC. Detailed examinations of the horizontal map for the temperature field further demonstrate that the warming temperature signals near the shelf break are closely linked to the intensified AW flow. These temperature anomalies near the shelf break help to strengthen the mean temperature front, resulting in a stronger eastward flow. On the other hand, the warming generated by the buoyancy experiment increases from the outer shelf toward the inner shelf. It is thus evident that both buoyancy and momentum fluxes contribute to temperature changes over the shallow waters, but momentum-driven process dominates those on the shelf break and deep ocean.

The response in salinity is rather different than that in temperature. The low-pass filtered salinity time series simulated by the momentum experiment closely follows that in the control run, and their correlation is about 0.72, significant at the 95% confidence level (Figure 11c). The salinity anomalies in both experiments range between −0.1 and 0.14. By contrast, interannual variations in salinity are weak in the buoyancy experiment and do not correlate with those in the control run (0.05). The vertical section for the salinity anomaly in 2003 reveals that large anomalies are found on the north Icelandic shelf in both the control and momentum experiments (Figure 13). In addition, the salinity anomalies in both experiments help to intensify the front near the shelf break. The salinity anomalies in the buoyancy run are very small almost everywhere along the section, suggesting that the surface buoycancy flux has little impact on the interannual salinity changes. River runoff is included in the model's forcing field. The freshwater input is only about 0.0048 Sv, and its role in salinity variability is negligible compared with the oceanic transport in this region (Jonsdottir 2008). Based on the AW volume fluxes in the momentum and buoyancy experiments and the salinity pattern shown in Figure 13, we conclude that the interannual changes for salinity along the Hornbanki section are primarily due to the advection of AW within the NIIC.

The zonal velocity anomalies along the Hornbanki section reveal the spatial structure for the maximum AW transport in 2003 (Figure 14). Both the control and momentum experiments generate significant velocity changes over the upper 300 m with elevated amplitude on the shelf, shelf break, and offshore part of the

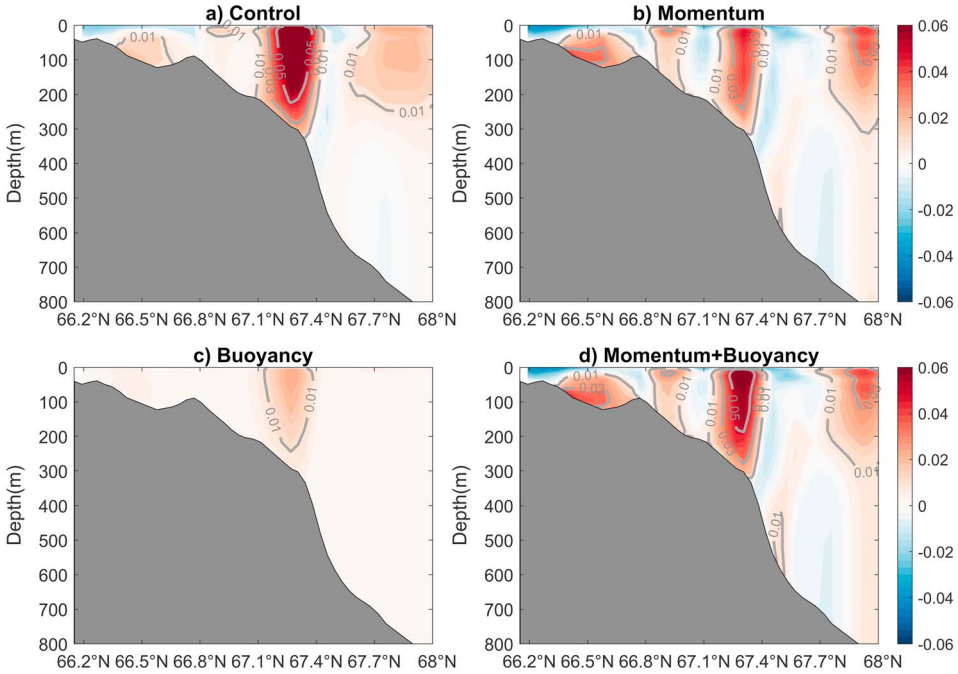

Figure 14. Same as Figure 12 except for the zonal velocity. (unit: m/s).

section. The velocity anomaly in the buoyancy run is mostly confined to the shelf break, which is induced by the buoyancy-forced warming signals over the shallow waters. Overall, the velocity responses are consistent with patterns in the temperature and salinity anomalies.

As discussed above, another important factor modulating the AW transport across the Hornbanki section is the relative proportion of AW and PW in the NIIC water. The AW proportion in each respective run is calculated independently using the time-varying end-member technique. The AW percentages in early 2003 are about 82% and 80% in control and momentum experiments, respectively. By contrast, the NIIC water in the buoyancy run only includes about 68% of the AW, which is the same level as in the climatological state. Therefore, the AW transport in the buoyancy run does not have an obvious increase in early 2003 (Figure 11a). This is the fundamental reason that the buoyancy run does not produce significant AW transport increase in the NIIC during the 2003 event.

The premise for comparing the control, momentum, and buoyancy experiments is that the physics for the AW interannual variability can be separated into *momentum-driven* and *buoyancy-driven* parts. Despite the inherently nonlinear nature of the ocean circulation, a linear superposition of changes from buoyancy and momentum forcing largely replicates the temperature, salinity, and velocity anomalies in the control experiment (Figures 12d, 13d, and 14d). This indicates that the dynamics governing the AW transport are predominantly linear.

It should be remembered that both the buoyancy and momentum runs include climatological seasonal components in their forcing fields. Consequently, they largely underestimate the responses due to high-frequency wind and buoyancy variations. As demonstrated by Logemann and Harms (2006), the short-term wind variations (time scales ranging from days to months) can drive NIIC high-frequency change. Therefore, caution should be taken when performing sensitivity experiments using climatological fields.

3.3. Atmospheric Forcing in 2003

To further identify regions where the momentum flux has the largest impact on the AW interannual variability, we computed the statistical correlation between the low-pass filtered AW transport in the control run and surface wind stress used in the model. The biggest interannual change, that is, the 2003 event, only lasted for several months; hence, it is difficult to use monthly time series to reveal

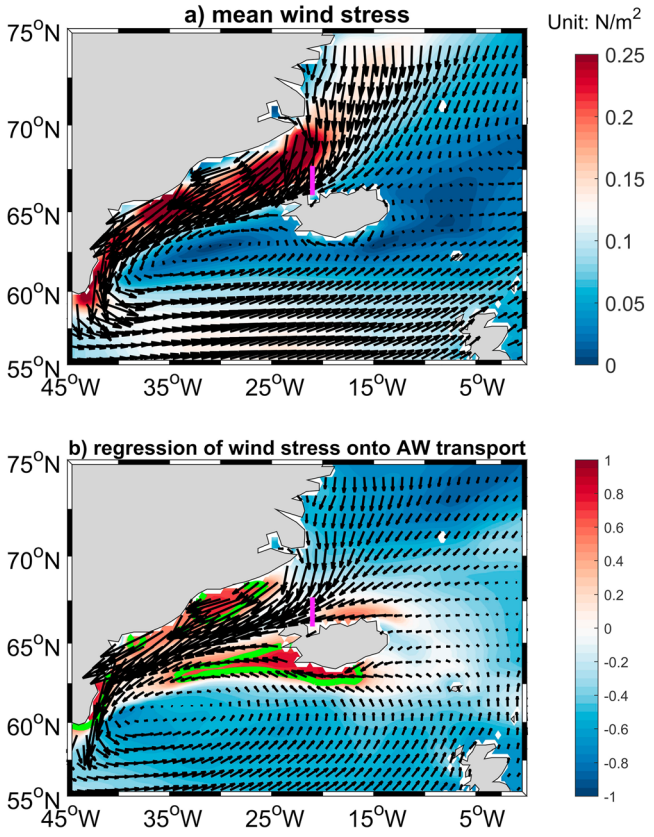

Figure 15. (a) Mean (1992–2015) surface wind stress vectors and magnitude (color shading) from the CFSR data set. (b) Regression of low-pass filtered wind stress onto the low-pass filtered AW transport in the control run. The correlation between the AW transport and the wind stress magnitude is displayed by the color shading. The green lines mark the regions where the confidence level exceeds 95% in the Student's *t* test. CFSR = Climate Forecast System Reanalysis; AW = Atlantic Water.

appropriate time lags between the atmospheric forcing and oceanic response during the 2003 event. Our aim therefore is to identify the geographical regions that affect the NIIC and its AW transport. The long-term mean surface wind stress exhibits a cyclonic circulation associated with the Icelandic Low (Figure 15a). The regressions of wind stress onto the AW transport leads to a spatial pattern that is quite similar to the long-term field (Figure 15b). The statistically important regions can be found from the correlation between the AW transport and the wind stress magnitude. The regions passing the 95% confidence level of the Student's *t* test are the eastern coast of Greenland, the northern Irminger Sea, and the area adjacent to southwest Iceland (denoted by green lines in Figure 15b).

The winds over these three regions reflect nonlocal (i.e., eastern coast of Greenland) and local forcing for the NIIC. For the nonlocal wind forcing, the special topographic structure near the Denmark Strait should be taken into consideration. The deep channel in the Denmark Strait has a water depth of 650 m, and the isobaths shallower than 650 m near Iceland are disconnected with those east of Greenland (Figures 9 and 10). This bathymetric feature makes it difficult to communicate the wind-driven signal east of Greenland to the north Icelandic shelf. Furthermore, the PW at the KG6 station does not show substantial interannual variability in temperature and salinity. Therefore, the wind forcing off Greenland is less likely to be responsible for changes of the AW transport at the Hornbanki section.

On the other hand, the increased southeasterly wind parallel to the southwest coast of Iceland leads to onshore Ekman transport and consequently produces northward geostrophic flow. The changes in pressure gradient and geostrophic velocity would propagate around Iceland and enhance the AW transport. Whether or not these processes are barotropic or baroclinic, their time scale is relatively short, usually less than 1 month (Richter et al., 2009). It is therefore difficult to capture them by lead-lag correlations using monthly data. In addition, the intensified easterly wind in the northern Irminger Sea would enhance the Irminger Current and hence increase the part that feeds the NIIC. Therefore, it appears more likely that the wind forcing southwest of Iceland and in the northern Irminger is responsible for the interannual variability of AW transport along the Hornbanki section.

To further elucidate the role of the wind field in the 2003 anomaly of AW transport in the NIIC, we examined the sea level pressure (SLP) field from the monthly NCEP-CFSR data set. The climatological mean SLP from January to April is constructed from the monthly data between 1992 and 2015. As shown in Figure 16a, the Icelandic Low is centered in the Irminger Sea, and in the Nordic Seas there is a signature of the Lofoten Low (in the northeasternmost part of the domain). By contrast, the mean SLP between January and April in 2003 indicates that the Icelandic Low deepened considerably and expanded into the Labrador Sea (Figure 16b). At the same time the low pressure in the Nordic Seas weakened. Taking the difference between the mean SLP in January–April 2003 and its corresponding climatological field yields the SLP anomaly pattern in early 2003 (Figure 16c). The SLP anomaly reveals a strong dipole, with a low centered near the southern tip of Greenland and a high located in the eastern Norwegian Sea. This large-scale SLP anomaly is associated with strengthened southeasterly winds off the southwest coast of Iceland, which in turn would result in more AW advected onto the north Icelandic shelf.

It is worth mentioning that our identification of wind changes southwest of Iceland is primarily based on statistical analysis. This does not entirely rule out the possibility of other factors to affect the AW volume transport in the NIIC. For example, the AW in the northern Icelandic shelf originates from the deep Irminger Sea. Any changes in the upper stream might affect the AW proportion in the NIIC. These processes could be subject of further study.

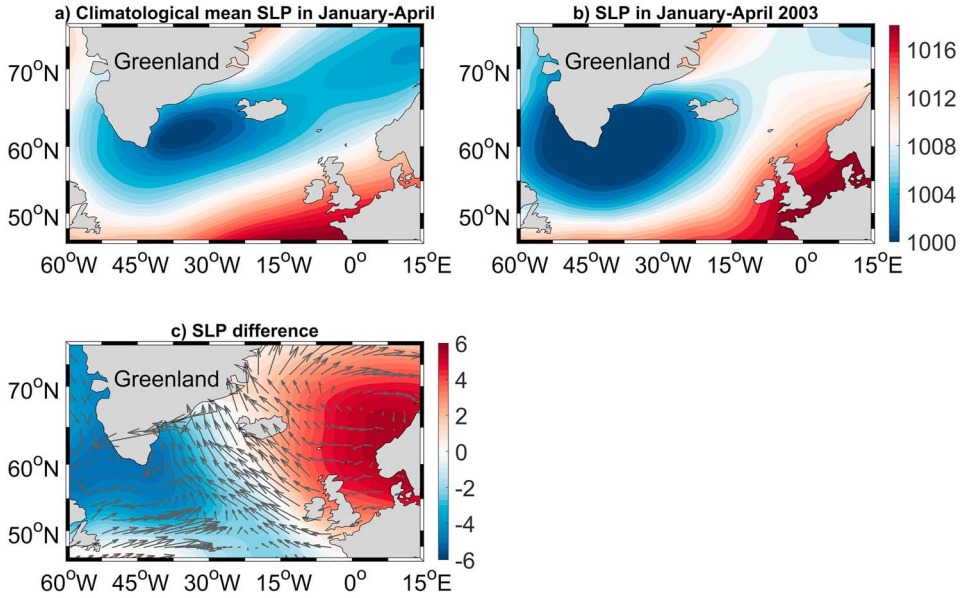

Figure 16. (a) Climatological mean sea level pressure (SLP) from January to April for the time period 1992–2015. (b) Mean SLP field between January and April 2003. (c) The 2003 mean field minus the climatological mean field. Unit: mbar. The gray vectors in Figure 16c illustrate the corresponding wind anomalies.

4. Summary and Discussion

In this study we have used the high-resolution HYCOM numerical model, together with various data sources, to investigate the seasonal to interannual variability of the NIIC and its AW transport. The mean hydrography and velocity structure along the Hornbanki section north of Iceland are well reproduced by HYCOM. Consistent with the observations, the model shows that the warm and salty water in the NIIC occupies the north Icelandic shelf and helps maintain a hydrographic front near the shelf break. The NIIC velocity profiles have both strong barotropic and baroclinic components. The core of the current is near the shelf break, corresponding to the density front.

The water mass in the NIIC is a mixture of AW and PW, and their ratios at the Hornbanki section were estimated using two end-member hydrographic profiles, as has been done in previous observational studies. The fraction of AW ranges from 50% to 95%, yielding a mean value of 72%. This value is slightly higher than the 68% obtained from the observations of Jónsson and Valdimarsson (2012). The mean AW transport in the model, as well as the simulated seasonal cycle and interannual variability, compares well with that from observations. This implies that the essential dynamics governing the flow of AW are well represented in the model.

The volume flux of AW in the NIIC varies considerably with season, from a minimum in late winter and early spring to a maximum in early fall. Variability in the relative percentages of the AW and PW contributes significantly to the NIIC seasonal cycle. The AW fraction changes seasonally in concert with the AW volume transport. The seasonal changes of the hydrographic structure over the entire north Icelandic shelf are in turn strongly modulated by this transport.

The most significant observed interannual change at the Hornbanki section in the two decades considered here occurred in 2003 and was related to the enhancement of the AW transport by the NIIC. This event is captured well in our control experiment. Two additional experiments were conducted to separate the impacts of buoyancy and momentum fluxes on the NIIC. Changes in wind stress alone, as shown in the momentum experiment, are largely responsible for the interannual variations in the AW volume transport and salinity. Variations in temperature, however, are attributed almost equally to changes in surface wind stress and buoyancy fluxes. Our analyses show that the two forcing fields affect the temperature through different processes. The wind-driven AW transport brings warm water onto the shelf and consequently impacts the temperature near the shelf break. The buoyancy forcing generates a temperature anomaly through surface forcing, with signals mainly located on the shelf and in the surface layer offshore.

Further statistical analyses between the AW volume transport and surface wind stress revealed that the wind stress southwest of Iceland seems to be primarily responsible for the interannual variability of the AW transport. Intensified southeasterly winds strengthen the NIIC transport of the AW to the north Icelandic shelf. This is consistent with the composite analyses conducted by Richter et al. (2009) who showed that the NIIC transport correlates positively with southerly wind anomalies around Iceland.

We also found that the southeasterly wind anomalies off Iceland in 2003 were associated with the large-scale SLP changes, that is, a dipole pattern with a low center in the Labrador Sea and Irminger Sea and a high center in the eastern Norwegian Sea. Interestingly, this dipole anomaly pattern is reminiscent of a leading mode of variability of the North Atlantic SLP field: the Scandinavian (SCA) pattern. Previous work pointed out that the interaction between the NAO and the SCA can result in movement of the Icelandic Low (Moore et al., 2013). We examined the NAO and SCA indices with an aim to understand why the SLP pattern in 2003 is unique over the last two decades. However, their indices indicate that both of them have several switches between positive and negative phases after the 1990s. If it was the combination of certain NAO and SCA phases that lead to the 2003 event, such event should have occurred several times after 1990. Apparently, future study is needed to further elucidate the connection between the wind pattern around Iceland and different modes of variability of the North Atlantic SLP.

Previous studies pointed out that the wind stress forcing is primarily responsible for salinity anomalies entering the Nordic Seas (Häkkinen et al., 2011; Hátún et al., 2005). Weakening cyclonic wind stress curl in the subpolar North Atlantic renders a westward shift of the subpolar front, so that more warm and saline subtropical waters penetrate farther north in the eastern part of the basin and hence increase the salinity in the inflow to the Nordic Seas. The most striking feature for the wind stress curl over the subpolar gyre is a decreasing trend starting from the 1990s. This qualitatively agrees with the increasing trend detected from the observed salinity time series along the Kögur section to the west of the Hornbanki line (Pickart et al., 2017). The numerical results in this study do not generate a long-term trend, at least not along the Hornbanki section. Instead, the most pronounced interannual changes are the increased AW transport and hydrographic signals in 2003. They are attributed to the wind forcing southwest of Iceland generated by the strengthening and westward shift of the Icelandic Low in early 2003. Although the local wind around Iceland is affected by the large-scale atmospheric pattern in the subpolar gyre, the different behaviors in the salinity time series suggest that the interannual variability discussed here is different from the long-term trend in the large-scale forcing.

Acknowledgments
This work is supported by the U.S. National Science Foundation (NSF) under grants OCE-1634886 (J. Zhao and J. Yang) and OCE-1558742 (R. Pickart), and by the Bergen Research Foundation grant BFS2016REK01 (K. Våge and S. Semper). We thank Xiaobiao Xu at Florida State University for providing the initial model configuration. Comments from anonymous reviewers help to improve the manuscript. The altimeter products are produced and distributed by the Copernicus Marine and Environment Monitoring Service (CMEMS, http://www.marine.copernicus.eu). The hydrographic maps along the Hornbanki section are available at http://www.hafro.is/Sjora/.

References

Astthorsson, O. S., Gislason, A., & Jonsson, S. (2007). Climate variability and the Icelandic marine ecosystem. *Deep Sea Research, Part II*, *54*(23-26), 2456–2477. https://doi.org/10.1016/j.dsr2.2007.07.030

Behrens, E., Våge, K., Harden, B., Biastoch, A., & Böning, C. W. (2017). Composition and variability of the Denmark Strait Overflow Water in a high-resolution numerical model hindcast simulation. *Journal of Geophysical Research: Oceans*, *122*, 2830–2846. https://doi.org/10.1002/2016JC012158

Berx, B., Hansen, B., Østerhus, S., Larsen, K., Sherwin, T., & Jochumsen, K. (2013). Combining in situ measurements and altimetry to estimate volume, heat and salt transport variability through the Faroe-Shetland channel. *Ocean Science*, *9*(4), 639–654. https://doi.org/10.5194/os-9-639-2013

Dickson, R., Meincke, J., & Rhines, P. (2008). *Arctic-Subarctic ocean fluxes* (p. 736). Dordrecht, Netherlands: Springer. https://doi.org/10.1007/978-1-4020-6774-7

Dickson, R. R., & Brown, J. (1994). The production of North Atlantic Deep Water: Sources, rates, and pathways. *Journal of Geophysical Research*, *99*(C6), 12,319–12,341. https://doi.org/10.1029/94JC00530

Häkkinen, S., Rhines, P. B., & Worthen, D. L. (2011). Warm and saline events embedded in the meridional circulation of the northern North Atlantic. *Journal of Geophysical Research*, *116*, C03006. https://doi.org/10.1029/2010JC006275

Hansen, B., Hátún, H., Kristiansen, R., Olsen, S. M., & Østerhus, S. (2010). Stability and forcing of the Iceland–Faroe inflow of water, heat, and salt to the Arctic. *Ocean Science*, *6*, 1245–1287.

Hansen, B., Larsen, K. M. H., Hátún, H., Kristiansen, R., Mortensen, E., & Østerhus, S. (2015). Transport of volume, heat and salt towards the Arctic in the Faroe Current 1993-2013. *Ocean Science*, *11*(5), 743–757. https://doi.org/10.5194/os-11-743-2015

Hansen, B., & Østerhus, S. (2000). North Atlantic–Nordic Seas exchanges. *Progress in Oceanography*, *45*(2), 109–208. https://doi.org/10.1016/S0079-6611(99)00052-X

Hansen, B., Østerhus, S., Ha'tu'n, H., Kristiansen, R., & Larsen, K. M. H. (2003). The Iceland-Faroe inflow of Atlantic water to the Nordic Seas. *Progress in Oceanography*, *59*, 443–474.

Hansen, B., Østerhus, S., Turrell, B., Jónsson, S., Valdimarsson, H., Hátún, H., et al. (2008). The inflow of Atlantic water, heat, and salt to the Nordic Seas across the Greenland-Scotland Ridge. In D. Dickson, J. Meincke & P. Rhines (Eds.), *Arctic–Subarctic ocean fluxes: Defining the role of the Northern Seas in climate* (Chap. 1, pp. 15–43). Dordrecht, Netherlands: Springer Science + Business Media B.V.

Hátún, H., Hansen, B., Sandø, A. B., Drange, H., & Valdimarsson, H. (2005). De-stabilization of the North Atlantic thermohaline circulation by a gyre mode. *Science*, *309*(5742), 1841–1844. https://doi.org/10.1126/science.1114777

Jakobsen, P. K., Ribergaard, M. H., Quadfasel, D., Schmith, T., & Hughes, C. W. (2003). Near-surface circulation in the northern North Atlantic as inferred from Lagrangian drifters: Variability from the mesoscale to interannual. *Journal of Geophysical Research*, *108*(C8), 3251. https://doi.org/10.1029/2002JC001554

Jónsdóttir, J. F. (2008). A runoff map based on numerically simulated precipitation and a projection of future runoff in Iceland. *Hydrological Sciences Journal*, *53*(1). https://doi.org/10.1623/hysj.53.1.100

Jónsson, S. (1999). The circulation in the northern part of the Denmark Strait and its variability, ICES CM, L:06, 9 pp

Jónsson, S., & Valdimarsson, H. (2004). A new path for the Denmark Strait Overflow Water from the Iceland Sea to Denmark Strait. *Geophysical Research Letters*, *31*, L03305. https://doi.org/10.1029/2003GL019214

Jónsson, S., & Valdimarsson, H. (2005). The flow of Atlantic water to the north Icelandic shelf and its relation to the drift of cod larvae. *ICES Journal of Marine Science*, *62*(7), 1350–1359. https://doi.org/10.1016/j.icesjms.2005.05.003

Jónsson, S., & Valdimarsson, H. (2012). Water mass transport variability to the north Icelandic shelf, 1994–2010. *ICES Journal of Marine Science*, *69*(5), 809–815. https://doi.org/10.1093/icesjms/fss024

Kara, A. B., Hurlburt, H. E., & Wallcraft, A. J. (2005). Stability-dependent exchange coefficients for air–sea fluxes. *Journal of Atmospheric and Oceanic Technology*, *22*, 1077–1091.

Logemann, K., & Harms, I. (2006). High resolution modelling of the North Icelandic Irminger Current (NIIC). *Ocean Science Discussions*, *3*(4), 1149–1189. https://doi.org/10.5194/osd-3-1149-2006

Moore, G. W. K., Renfrew, I. A., & Pickart, R. (2013). Multi-decadal mobility of the North Atlantic oscillation. *Journal of Climate*, *26*(8), 2453–2466. https://doi.org/10.1175/JCLI-D-12-00023.1

Nilsen, J. E. Ø., Gao, Y., Drange, H., Furevik, T., & Bentsen, M. (2003). Simulated North Atlantic–Nordic seas water mass exchanges in an isopycnic coordinate OGCM. *Geophysical Research Letters*, *30*(10), 1536. https://doi.org/10.1029/2002GL016597.

Olsen, S. M., & Schmith, T. (2007). North Atlantic-Arctic Mediterranean exchanges in an ensemble hindcast experiment. *Journal of Geophysical Research*, *112*, C04010. https://doi.org/10.1029/2006JC003838

Orvik, K. A., & Skagseth, Ø. (2003). The impact of the wind stress curl in the North Atlantic on the Atlantic inflow to the Norwegian Sea toward the Arctic. *Geophysical Research Letters*, *30*(17), 1884. https://doi.org/10.1029/2003GL017932

Østerhus, S., Turrell, W. R., Jonsson, S., & Hansen, B. (2005). Measured volume, heat, and salt fluxes from the Atlantic to the Arctic Mediterranean. *Geophysical Research Letters*, *32*, L07603. https://doi.org/10.1029/2004GL022188

Pickart, R. S., Spall, M. A., Torres, D. J., Vage, K., Valdimarsson, H., Nobre, C., et al. (2017). The North Icelandic Jet and its relationship to the North Icelandic Irminger Current. *Journal of Marine Research*, *75*(5), 605–639. https://doi.org/10.1357/002224017822109505

Richter, K., Furevik, T., & Orvik, K. A. (2009). Effect of wintertime low pressure systems on the Atlantic inflow to the Nordic Seas. *Journal of Geophysical Research*, *114*, C09006. https://doi.org/10.1029/2009JC005392

Richter, K., Segtnan, O., & Furevik, T. (2012). Variability of the Atlantic inflow to the Nordic Seas and its causes inferred from observations of sea surface height. *Journal of Geophysical Research*, *117*, C04004. https://doi.org/10.1029/2011JC007719

Saha, S., Moorthi, S., Pan, H.-L., Wu, X., Wang, J., & Nadiga, S. (2010). The NCEP Climate Forecast System Reanalysis. *Bulletin of the American Meteorological Society*, *91*(8), 1015–1058. https://doi.org/10.1175/2010BAMS3001.1

Saha, S., Moorthi, S., Wu, X., Wang, J., Nadiga, S., & Tripp, P. (2014). The NCEP Climate Forecast System version 2. *Journal of Climate*, *27*(6), 2185–2208. https://doi.org/10.1175/JCLI-D-12-00823.1

Sandø, A. B., & Furevik, T. (2008). Relation between the wind stress curl in the North Atlantic and the Atlantic inflow to the Nordic Seas. *Journal of Geophysical Research*, *113*, C06028. https://doi.org/10.1029/2007JC004236

Sandø, A. B., Nilsen, J., Eldevik, T., & Bentsen, M. (2012). Mechanisms for variable North Atlantic-Nordic Seas exchanges. *Journal of Geophysical Research*, 117, C12006. https://doi.org/10.1029/2012JC008177

Santer, B. D., Wigley, T. M. L., Boyle, J. S., Gaffen, D. J., Hnilo, J. J., Nychka, D., et al. (2000). Statistical significance of trends and trend differences in layer average atmospheric temperature time series. *Journal of Geophysical Research*, *105*(D6), 7337–7356. https://doi.org/10.1029/1999JD901105

Sherwin, T. J., Hughes, S. L., Turrell, W. R., Hansen, B., & Østerhus, S. (2008). Wind-driven monthly variations in transport and the flow field in the Faroe-Shetland channel. *Polar Research*, *27*(1), 7–22. https://doi.org/10.1111/j.1751-8369.2007.00036.x

Thordardottir, Th. (1984). Primary production north of Iceland in relation to water masses in May–June 1970–1980. ICES Document CM 1984/L: 20.17 pp.

Våge, K., Pickart, R. S., Spall, M. A., Valdimarsson, H., Jonsson, S., Torres, D. J., et al. (2011). Significant role of the North Icelandic Jet in the formation of Denmark Strait Overflow Water. *Nature Geoscience*, *4*(10), 723–727. https://doi.org/10.1038/ngeo1234

Våge, K., Pickart, R. S., Spall, M. A., Moore, G. W. K., Valdimarsson, H., Torres, D. J., et al. (2013). Revised circulation scheme north of the Denmark Strait. *Deep Sea Research, Part I*, *79*, 20–39.

Valdimarsson, H., & Malmberg, S.-A. (1999). Near-surface circulation in Icelandic waters derived from satellite tracked drifters. *Rit Fiskideildar*, *16*, 23–39.

Xu, X., Hurlburt, H. E., Schmitz, W. J. Jr., Fischer, J., Zantopp, R., & Hogan, P. J. (2013). On the currents and transports connected with the Atlantic meridional overturning circulation in the subpolar North Atlantic. *Journal of Geophysical Research: Oceans*, *118*, 502–516. https://doi.org/10.1002/jgrc.20065

Xu, X., Schmitz, W. J. Jr., Hurlburt, H. E., & Hogan, P. J. (2012). Mean Atlantic meridional overturning circulation across 26.5°N from eddy-resolving simulations compared to observations. *Journal of Geophysical Research*, *117*, C03042. https://doi.org/10.1029/2011JC007586

Xu, X., Schmitz, W. J. Jr., Hurlburt, H. E., Hogan, P. J., & Chassignet, E. P. (2010). Transport of Nordic Seas overflow water into and within the Irminger Sea: An eddy-resolving simulation and observations. *Journal of Geophysical Research*, *115*, C12048. https://doi.org/10.1029/2010JC006351